# A newly developed screening current simulation method for REBCO pancake coils based on extension of PEEC model

**So Noguchi**[1] **and Seungyong Hahn**[2]

[1] Graduate School of Information Science and Technology, Hokkaido University, Sapporo 060-0814, Japan

[2] Department of Electrical and Computer Engineering, Seoul National University, Seoul 08826, Republic of Korea

E-mail: noguchi@ssi.ist.hokudai.ac.jp

August 2021

**Abstract.** Since the screening current (SC) in rare earth-barium-copper-oxide (REBCO) coated conductor (CC) generates an undesired magnetic field, it must be accurately estimated, especially for magnetic resonance imaging (MRI) and nuclear magnetic resonance (NMR). Moreover, in recent years, it was pointed out that the screening current enhanced the stress/strain in REBCO CC, when an REBCO magnet was operated as an insert under an ultrahigh magnetic field. The previously reported SC simulation methods may be roughly categorized into finite element method (FEM) and equivalent circuit method. The FEM-based method often adopted an axisymmetric model or a thin film approximation model, while the circuit-based are the simple equivalent circuit model and the network equivalent circuit model, so-called the partial element equivalent circuit (PEEC) model. The latter is newly developed in this paper. Features of those SC simulation models are briefly compared to each other in this paper. Each SC simulation models have pros & cons. We have to adequately chose an SC simulation model depending on a purpose.

We extended the original PEEC model to simulate SC. The extended model is named the advanced partial element equivalent circuit (A-PEEC) model. It is also extendable to an SC simulation of no-insulation REBCO pancake coils. To simulate the SC of a simple coil model and the LBC3 magnet, we investigated the screening current distribution maps, and the simulated screening current-induced fields were compared with the measurements. We have confirmed the validity of the newly developed A-PEEC model.

## 1. Introduction

Higher magnetic fields are often desired in various applications including magnetic resonance imaging (MRI) [1, 2, 3], nuclear magnetic resonance (NMR) [4, 5, 6, 7], and particle accelerators [8, 9, 10, 11]. Rare earth-barium-copper-oxide (REBCO) coated conductor (CC) has been regarded as a promising conductor option for ultrahigh

magnetic field superconducting magnets. Meanwhile, the screening current (SC) induced in the REBCO CCs generates an undesired magnetic field [12, 13, 14, 15]. Recently, it was pointed out that the screening current may substantially enhance magnetic stress in REBCO magnets [16, 17, 18, 19, 20, 21]. To estimate the peak stress accurately, the importance of the accurate computation of the screening current distribution must be enhanced. To protect high-field HTS magnet from excessive stress concentration, the screening current behaviors have been discussed [22].

So far, a few screening current simulation methods have been proposed, which include: (1) an axisymmetric finite element method (Axi-FEM) [23, 24]; (2) a finite element method with a thin film approximation technique (FEM+TFA) [15, 25, 26, 27, 28]; (3) a simple equivalent circuit (SEC) model [29]; and (4) an advanced partial element equivalent circuit (A-PEEC) model which is shown for an SC simulation in this paper.

The Axi-FEM and the FEM+TFA are a FEM-based model, in which a special technique needs to be coupled with FEM to deal with the air region or to accelerate the computation. Berrospe-Juarez, *et al.* proposed a special technique using multi-scale and homogenization technique in order to simulate a large-scale REBCO magnet with the COMSOL Multiphysics software [30]. Meanwhile, in the conventional Axi-FEM, to obtain a high spatial resolution of screening current distribution, the REBCO layers are subdivided into fine meshes. The SEC and the A-PEEC are based on the equivalent circuit approach. In these models, since inductances are used in an equivalent circuit, fine meshes of the air region is unnecessary, while a larger number of elements in the REBCO region often helps to improve the simulation accuracy with a reasonably short computation time. It is possible to choose a SC computation method depending on the user's target. The Axi-FEM would be superior to the computation time and the convenience, because it works on the COMSOL Multiphysics software, and it was reported that it could give accurate solutions [22, 23, 24].

This paper provides a brief summary of key feature of those aforementioned SC simulation methods with comparison among simulation results by each simulation approach. In addition, a new concept of the SC simulation model, A-PEEC, is mentioned in this paper. While the SEC and the Axi-FEM employ a simplified model, the FEM+TFA model brings an accurate solution due to fine mesh. The FEM+FEA model is a time-consuming method without using a special technique. Therefore, we developed a circuit-based model (A-PEEC) with a high spatial resolution based on a simple principle. The PEEC or network model was proposed and applied to many cases for investigation of the magnet stability [31, 32, 33, 34, 35]. In this paper, we propose the extension of the conventional PEEC model to compute the screening current by tape-transversely subdividing a REBCO tape to some elements. The developed A-PEEC model is applicable to a no-insulation (NI) REBCO pancake coils. Finally, we simulated the screening current-induced fields for two REBCO magnets, together with a comparison with the measurements. In the near future, the A-PEEC can apply the thermal stability computation of NI REBCO magnets by coupling the thermal analysis.

In this moment, it is hard to investigate the effect of the screening current on the thermal stability of NI REBCO magnets.

## 2. Brief Overview of Three Kinds of SC Simulation Models

Figure 1 summarizes key concepts of the three screening current (SC) simulation methods, of which individual features are described below.

### *2.1. Axisymmetric FEM (Axi-FEM)*

In Axi-FEM [23, 24], the current phenomenon is considered on the axisymmetric $r$-$z$ plane. The governing equation of $A$ method is:

$$\frac{\partial}{\partial z}\left(\frac{1}{\mu}\frac{\partial A_\theta}{\partial z}\right)+\frac{\partial}{\partial r}\left(\frac{1}{r\mu}\frac{\partial A_\theta}{\partial r}\right)=\left(\sigma\frac{\partial A_\theta}{\partial t}+J_{\rm op}\right) \tag{1}$$

where $A_\theta$, $\mu$, $\sigma$, and $J_{\rm op}$ are, respectively, the magnetic vector potential in the $\theta$ component, the magnetic permeability, the electric conductivity, and the operating current density. Commonly, $rA$ is the unknown variables to be solved in order to avoid singularity at the axis of the symmetry. To compute $J_{\rm op}$, the gradient of scalar potential must be introduced [36].

Using only the $A$ method, it is difficult to solve the screening current distribution of multi-stacked pancake coils with many turns. Berrospe-Juarez, *et al.* proposed a method coupling with $T$ formulation. The equation of $T$ formulation in [30] is derived in 2-D space by neglecting the thickness of REBCO layers, as follows:

$$\frac{\partial}{\partial x}\left(\rho_{\rm HTS}\frac{\partial T_y}{\partial x}\right)=\frac{B_y}{\partial t} \tag{2}$$

where $\rho_{\rm HTS}$, $T_y$, and $B_y$ are the REBCO resistivity and the current vector potential, and the magnetic flux density, respectively. Here, $x$ and $y$ are coordinates in the tape width and thickness directions, respectively. This method is called the $T$-$A$ formulation, which has been widely used nowadays.

In Axi-FEM, currents in the axial component are neglected at the REBCO tape ends. And, it is impossible to consider the spiral pancake-winding structure and the inductive current by the time-varying axial field in (2). However, in [24], Mataira, *et al.* have proposed a method to consider the spiral pancake-winding structure and the no-insulation (NI) winding based on the $H$-formulation.

### *2.2. FEM with Thin Film Approximation (FEM+TFA)*

In FEM+TFA [15, 25, 26, 27, 28], only the REBCO layer or tape is subdivided into fine meshes, and the governing equation is given as:

$$\begin{aligned}&\{\nabla\times\rho(\nabla T\times\boldsymbol{n})\}\cdot\boldsymbol{n}\\&+\frac{\mu d}{4\pi}\frac{\partial}{\partial t}\int_s\frac{(\nabla T'\times\boldsymbol{n}')\times\boldsymbol{R}}{|\boldsymbol{R}|^3}{\rm d}s'=-\frac{\partial\boldsymbol{B}_0}{\partial t}\cdot\boldsymbol{n}\end{aligned} \tag{3}$$

where $T$, $\rho$, $\boldsymbol{n}$, $d$, $\boldsymbol{R}$, and $\boldsymbol{B}_0$ are the current vector potential, the electric resistivity, the unit vector perpendicular to the wide surface of REBCO tape, the REBCO layer thickness, the distance vector from the current source to the field point, and the external magnetic field, respectively. The second term in the left side is derived according to the thin film approximation [37, 38]. The matrix to be solved is full because of the second term in the left side. To effectively solve the matrix, a special technique is used such as a fast multipole method [39, 40]

As seen in (3), the time-varying radial field is considered, while the time-varying axial field is neglected. In the FEM+TFA, although the REBCO tape thickness is considered at the second term in the left side of (3) to compute the magnetic field, the REBCO tape is, actually, approximated with infinite thickness for the time-varying axial field [27]. According to the paper [41], the time-varying axial field affects the current distribution.

### *2.3. Simple Equivalent Circuit (SEC)*

The screening current behaviors may be represented with multiple inductive components [42]. Coupling the screening current equivalent circuit to an NI equivalent circuit [43, 44], it is possible to simulate the screening current of NI pancake coils as well as conventional insulated pancake ones [29]. The following circuit equations are solved in the SEC model:

$$L\frac{\mathrm{d}I_\theta}{\mathrm{d}t} + M\frac{\mathrm{d}I_{sc}}{\mathrm{d}t} + \frac{R_{\mathrm{re}}R_{\mathrm{mt}}}{R_{\mathrm{re}}+R_{\mathrm{mt}}}I_\theta = R_{\mathrm{ct}}(I_{\mathrm{t}} - I_\theta) \tag{4}$$

$$L\frac{\mathrm{d}I_{\mathrm{sc}}}{\mathrm{d}t} + M\frac{\mathrm{d}I_\theta}{\mathrm{d}t} = R_{\mathrm{sc}}I_{\mathrm{sc}} \tag{5}$$

where $L$, $M$, $R_{\mathrm{re}}$, $R_{\mathrm{mt}}$, $R_{\mathrm{ct}}$, and $R_{\mathrm{sc}}$ are the self and mutual inductances, and the resistances of REBCO layer, copper matrix, turn-to-turn contact, and the screening current, respectively. $I_\theta$, $I_{\mathrm{sc}}$, and $I_{\mathrm{t}}$ are the azimuthal coil current, the radial turn-to-turn contact current, and the source current, respectively.

In the SEC model, the mutual inductances include the effect of the magnetic field change in the axial and radial components. Since a pancake coil is not subdivided into elements and the screening current path is assumed to be on the top and bottom of coil, the simulation accuracy may not be good. In addition, the axial current at the tape ends and the spiral structure cannot be taken into account. The SEC model is the best way to roughly estimate the screening current-induced fields with a relatively short computation time, and it can deal with not only turn-insulated pancake coils but NI ones.

### *2.4. Brief Overview of Simulation Models*

Key features of each simulation method of screening currents are summarized in table 1. When a complete 3-D FEM is employed, a fine mesh is needed to accurately simulate the screening current. Since mesh generation in a full 3-D space is computationally expensive

due to thin REBCO tape thickness, some assumptions are often made; *e.g.*, axisymmetry or thin film approximation. Because of these assumptions, the Axi-FEM cannot consider the axial current and the pancake winding structure, and the FEM+TFA cannot take into account the current induced by the time-varying axial field. However, the Axi-FEM has a good balance between the computation time and the solution accuracy.

The SEC model is too simple to accurately simulate the screening current, because much phenomena are simplified.

## 3. Developed Screening Current Simulation Model (Advanced Partial Element Equivalent Circuit Model)

As mentioned in the previous chapter, the FEM-based models have some assumptions, and the model accuracy is deteriorated. To overcome such problems, we propose a circuit-based model, which has no assumption and does not need mesh generation like FEM. The developed method can consider the pancake winding structure, the axial current, and the time-varying axial field.

Previously, the complicated equivalent circuit models, *e.g.*, a partial element equivalent circuit (PEEC) model [31, 32] and a network model [33, 34], has been proposed for simulation of an NI pancake coil. We propose a new concept to simulate screening currents; *i.e.*, the PEEC model is extendable to the REBCO tape transverse direction for a screening current simulation, named an advanced PEEC (A-PEEC) model, as shown in figure 2. Figure 3 shows some local loops in the A-PEEC model, of which the governing equations are given as

$$\begin{aligned}&\sum_{i=1}^{m} L_{l,i}\frac{\mathrm{d}I_i}{\mathrm{d}t} + R_l I_l + \sum_{j=1}^{n} L_{t,j}\frac{\mathrm{d}I_j}{\mathrm{d}t} + R_t I_t \\ &= \sum_{i=1}^{m} L_{l+1,i}\frac{\mathrm{d}I_i}{\mathrm{d}t} + R_{l+1} I_{l+1} + \sum_{j=1}^{n} L_{t+1,j}\frac{\mathrm{d}I_j}{\mathrm{d}t} + R_{t+1} I_{j+1} \\ &(l = 1, \cdots, m, \quad t = 1, \cdots, n)\end{aligned} \tag{6}$$

$$\begin{aligned}&\sum_{i=1}^{m} L_{l,i}\frac{\mathrm{d}I_i}{\mathrm{d}t} + R_l I_l + R_g I_g = \sum_{i=1}^{m} L_{l+1,i}\frac{\mathrm{d}I_i}{\mathrm{d}t} + R_{l+1} I_{l+1} + R_{g+1} I_{g+1} \\ &(l = 1, \cdots, m)\end{aligned} \tag{7}$$

$$\begin{aligned}&I_l + I_{l+1} + I_t + I_{t+1} + I_g + I_{g+1} = 0 \\ &(l = 1, \cdots, m, \quad t = 1, \cdots, n)\end{aligned} \tag{8}$$

where $I$, $L$, and $R$ are the current, the inductance, and the resistance, respectively. $m$ and $n$ are the tolal division number of the tape-longitudinal and transverse directions. The sufixews $o$ is the number of contact resistances, and $p$ is the number of pancake coils whose inductance is considered as a whole. The subscripts $l$, $t$, and $g$ means the tape-longitudinal, tape-transverse, and coil-radial direction,. When this model is applied to an insulated REBCO pancake coil, the terms of contact resistances $R_g$ are omitted.

As good features of the A-PEEC model, it is possible to consider the axial current at the tape ends, the spiral pancake-winding structure, and the time-varying axial magnetic field. It is also applicable to simulation of the NI pancake coils. However, the inductance computation in the A-PEEC model is quite complicated and requires substantial computation time. Moreover, when the element is very small, it is difficult to compute accurate inductances. The self-inductances used in this paper were obtained according to [45] with a great number of nodes of Gauss-Legendre quadrature:

$$L = \frac{1}{I^2}\int \boldsymbol{A}(\boldsymbol{x})\cdot\boldsymbol{J}(\boldsymbol{x})dv \tag{9}$$

$$\boldsymbol{A}(\boldsymbol{x}) = \frac{\mu_0}{4\pi}\int \frac{\boldsymbol{J}(\boldsymbol{x'})}{|\boldsymbol{x}-\boldsymbol{x'}|}dv' \tag{10}$$

where $I$, $\boldsymbol{J}$, $\mu_0$, $\boldsymbol{x}$, and $\boldsymbol{x'}$ are, respectively, the current, the current density, the permeability of free space, the position vectors in the coil volume $v$ dnd $v'$. To avoid zero division in the Gauss-Legendre quadrature, the different number of Gauss nodes of (9) and (10) must be employed. In this paper, 70 and 25 nodes are adopted for (9) and (10), respectively. The following equations are the mutual inductance $M_{12}$ between partial elements 1 and 2:

$$M_{12} = \frac{E_m - \frac{1}{2}L_1I_1^2 - \frac{1}{2}L_2I_2^2}{I_1I_2} \tag{11}$$

$$E_m = \frac{1}{2}\int \boldsymbol{A}(\boldsymbol{x}_1)\cdot\boldsymbol{J}(\boldsymbol{x}_1)dv_1 + \frac{1}{2}\int \boldsymbol{A}(\boldsymbol{x}_2)\cdot\boldsymbol{J}(\boldsymbol{x}_2)dv_2 \tag{12}$$

$$\boldsymbol{A}(\boldsymbol{x}_i) = \frac{\mu_0}{4\pi}\left\{\int \frac{\boldsymbol{J}(\boldsymbol{x'}_i)}{|\boldsymbol{x}_i-\boldsymbol{x'}_i|}dv'_i + \int \frac{\boldsymbol{J}(\boldsymbol{x'}_j)}{|\boldsymbol{x}_j-\boldsymbol{x'}_j|}dv'_j\right\} \tag{13}$$

where $(i,j) = (1,2)$ or $(2,1)$. To accurately compute the mutual inductances, 70 and 25 nodes are also employed for (12) and (13).

The FEM-based methods have a high spatial resolution; while the circuit-based methods are highly expandable and flexible, *e.g.*, applicable to simulation of NI REBCO coils.

## 4. Simulation Results

The simulation results of the proposed A-PEEC are shown below, applying to two REBCO magnets: (1) a simple REBCO magnet consisting of 2 double- and 4 single-pancake (2 DP + 4 SP) coils with turn-to-turn insulation [29, 42, 46], and (2) a 14-T no-insulation (NI) REBCO insert magnet, named LBC3 [16], which generated 14.4 T inside a background field of 31.1 T. The simulated screening current-induced fields of both cases are compared with the measured ones.

### *4.1. A Simple Model (2 DP + 4 SP Coils)*

To compare the SC simulation models with experiments, a simple magnet consisting of 2 double (DP) and 4 single pancake (SP) coils [figure 4(a)] [46] are simulated. In order to measure the screening current-induced fields (SCIF), this simple model coil was manufactured in several years ago. We measured the time-transient SCIFs, and we simulated the SCIF with the FEM+TFA and the SEC. Table 2 lists key parameters of the coils. The measured coil critical currents ($I_c$) and $n$ value measured in liquid nitrogen are also shown in table 2. The magnet was linearly charged at a ramping rate of 3 A·min$^{-1}$, as shown in figure 4(b). As the $E$-$J$ relation depends on the magnetic field, the power index model presented in [47] is employed.

#### *4.1.1. Screening Current-Induced Field*

Figure 5 shows the screening current-induced fields at the magnet center, both the measurement and the simulation results of FEM+TFA, SEC, and A-PEEC. The results of FEM+TFA and SEC were presented in [29]. Here, the screening current-induced field $B_{sc}$ is defined as

$$B_{sc}(I_{op}) = B_0(I_{op}) - \alpha I_{op} \tag{14}$$

where $B_0(I_{op})$ is measured or simulated axial field at magnet center, $I_{op}$ operating current, and $\alpha$ coil constant obtained by measuring a magnetic field with application of a small current in the normal state without screening current considered.

The A-PEEC simulation result are close to the measurement. The screening current-induced fields of FEM+TFA and SEC are somehow overestimated.

#### *4.1.2. Current Distribution Maps*

Figure 6 shows the time transition of current distribution obtained with the A-PEEC model. At the beginning of charging ($I_{op} = 10$ A), the negative current can be observed on the bottom of SP 3 and the upper SP of DP 1. The current density increases all over the entire coils during charging, mainly because the time-varying axial field is considered in a similar way reported in the Norris's paper [41]. It is noticed that the average current density in the REBCO layer thickness direction is depicted in figure 6. This model does not have a spatial resolution enough to express a local current density in the REBCO layer thickness direction. Eventually, the increase in the current all over the entire coils reduces the screening current-induced field at the magnet center. Especially, from 20 to 30 A, the SCIF changes to flatten. This phenomenon is different form that of the other models. Figure 7 shows the ratio of the screening current density to the critical current density at $I_{op} = 30$ A. The screening current density of DP 1 is almost the critical current density; however, the screening current of SP 3 does not reach the critical current density. This is the cause of the flat SCIF between 20 and 30 A.

### *4.2. 14-T NI REBCO Insert Magnet (LBC3)*

The second simulated magnet is an NI REBCO insert magnet (LBC3) [16]. Although the turn-to-turn of the first simulated magnet was insulated, the proposed method can apply to NI magnets. However, it is difficult to estimate the SCIF accurately, because NI magnets have a charging delay. In this paper, the computed magnetic field is compared with the measured field including the SCIF and the charging delay.

The LBC3 magnet consists of 12 single pancake coils without turn insulation, and figure 8(a) shows the LBC3 magnet configuration. Table 3 lists the outline specifications of the LBC3, and the details are given in [16, 42]. The current linearly increases up to 50 A with 0.5 A·s$^{-1}$, and then it stays at 50 A for 50 s [figure 6(b)]. In the simulations, two cases were conducted: (1) turn insulation (INS) and (2) no-insulation (NI) with the turn-to-turn contact resistivity of 7 $\mu\Omega$·cm$^2$ [42]. Any external magnetic field is not applied to the LBC3 magnet as an LBC3 standalone test.

Figure 9 shows the axial magnetic field at the magnet center in the both cases of INS and NI. The axial field linearly rises up to 2.80 T in the case of INS, meanwhile a charging delay is observed in the case of NI. Finally, the last axial field of NI reaches to the same value as that of INS.

The measured axial fields at the operating currents $I_{\mathrm{op}} = 8.96$ and 48.9 A are shown in table 4. The measurements are close to the computed fields of both INS and NI cases. In this paper, the contact resistivity measured in the preliminary experiment was used. However, it may vary because of the hoop-stress change in high field.

Figures 10 shows the time-transient current distribution maps of NI. The current density inside each pancake coil linearly increases from 25 s to 100 s. The SPs 1, 2, 11, and 12 have a large screening currents. Such large screening currents generate over-estimated stress [17]. In the near future, we have to simulate the stress using this simulated SCIF.

In addition, to investigate the thermal stability NI magnet, it is also necessary to couple the A-PEEC method with a thermal analysis, together with the consideration of the magnet deformation [22].

## 5. Conclusion

In this paper, four numerical models to simulate screening current (SC) in REBCO coils are briefly studied: (1) the axisymmetric FEM (Axi-FEM); (2) FEM with the thin film approximation (FEM+TFA); (3) the simple equivalent circuit (SEC) model; and (4) the advanced partial element equivalent circuit (A-PEEC) model. The A-PEEC is newly developed for SC simulation, because the circuit-based model has many good features when compared to the FEM-based models. The A-PEEC has many features which cannot be considered by the other models; (1) the induction by the time-varying axial field; (2) the spiral pancake-winding structure; (3) the axial current; and (4) the

applicability to NI REBCO pancake. The each model has different characters. We have to choose an adequate model to our simulation aim. Although the FEM+FEA is an accurate method, its computational load is high. Meanwhile, the variety of Axi-FEM were proposed, and many researchers use it.

In this paper, considering the characteristics of the above methods, we proposed the A-PEEC method. The A-PEEC method was developed based on the PEEC model, which has already been used for the investigation of NI magnet stability. To confirm the validity of the A-PEEC method, the SC distributions of the simple test magnet and the LBC3 magnet were computed. The screening current-induced fields obtained by the A-PEEC were compared with the measurements. The first test model is an turn-to-turn insulated magnet. Since we have the time-transient SCIF measurements, the simulation results are compared with them. The second model (LBC3 magnet) is an NI magnet. Since the proposed A-PEEC model is applied to NI magnets, we computed and compare the SCIF of the LBC3 magnet with the measurement. In near future, we will develop the proposed method so that the thermal stability of NI magnets is evaluated as well as the coil deformation by stress analysis. The screening current affect the coil deformation, and the coil deformation would change the contact resistivity which is an important stability factor of NI magnet.

## Acknowledgement

This work was supported in part by the JSPS KAKENHI under Grant No. 20H02125.

## References

[1] Tosaka T, Miyazaki H, Iwai S, Otani Y, Takahashi M, Tasaki K, Nomura S, Kurusu T, Ueda H, Noguchi S, Ishiyama A, Urayama S and Fukuyama H 2016 R&D project on HTS magnets for ultrahigh-field MRI systems *IEEE Trans. Appl. Supercond.* **26** 4402505.

[2] Miyazaki H, Iwai S, Otani Y, Takahashi M, Tosaka T, Tasaki K, Nomura S, Kurusu T, Ueda H, Noguchi S, Ishiyama A, Urayama S and Fukuyama H 2016 Design of a conduction-cooled 9.4T REBCO magnet for whole-body MRI systems *Supercond. Sci. Technol.* **29** 104001.

[3] Yokoyama S, Lee J, Imura T, Matsuda T, Eguchi R, Inoue T, Nagahiro T, Tanabe H, Sato S, Daikoku A, Nakamura T, Shirai Y, Miyagi D and Tsuda M 2017 Research and development of the high stable magnetic field ReBCO coil system fundamental technology for MRI *IEEE Trans. Appl. Supercond.* **27** 4400604

[4] Iwasa Y, Bascuñán J, Seungyong H, Voccio J, Kim Y, Lécrevisse T, Song J and Kajikawa K 2015 A high-resolution 1.3-GHz/54-mm LTS/HTS NMR magnet *IEEE Trans. Appl. Supercond.* **25** 4300205

[5] Noguchi S, Park D, Choi Y, Lee J, Li Y, Michael P C, Basucuñán J, Hahn S and Iwasa Y 2019 Quench analyses of the MIT 1.3GHz LTS/HTS NMR magnet *IEEE Trans. Appl. Supercond.* **29** 4301005

[6] Park D, Bascuñán J, Michael P C, Lee J, Choi Y H, Li Y, Hahn S and Iwasa Y, 2019 MIT 1.3-GHz LTS/HTS NMR magnet: post quench analysis and new 800-MHz insert design *IEEE Trans. Appl. Supercond.* **29** 4300804

[7] Iguchi S, Piao R, Hamada M, Matsumoto S, Suematsu H, Takao T, Saito A T, Li J, Nakagome, H, Jin X, Takahashi M, Maeda H and Yanagisawa Y 2016 Advanced field shimming technology to

reduce the influence of a screening current in a REBCO coil for a high-resolution NMR magnet *Supercond. Sci. Technol.* **29** 045013

[8] Ueda H, Fukuda M, Hatanaka K, Wang T, Wang X, Ishiyama A, Noguchi S, Nagaya S, Kashima N and Miyahara N 2013 Conceptual design of next generation HTS cyclotron *IEEE Trans. Appl. Supercond.* **23** 4100205.

[9] Nugteren J, Kirby G, Murtomäki J, DeRijk G, Rossi L and Stenvall A 2018 Toward REBCO 20 T+ dipoles for accelerators *IEEE Trans. Appl. Supercond.* **28** 4008509.

[10] Takayama S, Iwai S, Kubo Y, Koyanagi K, Miyazaki H, Orikasa T, Ishii Y, Kurusu T, Amemiya N, Ogitsu T, Iwata Y, Noda K and Yoshimoto M 2019 Development of an HTS accelerator magnet with REBCO coils for tests at HIMAC beam line *IEEE Trans. Appl. Supercond.* **29** 4004205.

[11] Ueda H, Ishiyama A, Noguchi S, Watanabe T, Nagaya S, Yoshida J and Fukuda M 2019 Conceptual design of compact HTS cyclotron for RI production *IEEE Trans. Appl. Supercond* **29** 4101105.

[12] Miyazaki H, Iwai S, Uto T, Otani Y, Tkahashi M, Tosaka T, Tasaki K, Nomura S, Kurusu T, Ueda H, Noguchi S, Ishiyama A, Urayama S and Fukuyama H 2017 Screening-current-induced magnetic field of conduction-cooled HTS magnets wound with REBCO-coated conductors *IEEE Trans. Appl. Supercond.* **27** 4701705.

[13] Uglietti D, Yanagisawa Y, Maeda H and Kiyoshi T 2010 Measurements of magnetic field induced by screening currents in YBCO solenoid coils *Supercond. Sci. Technol.* **23** 115002.

[14] Dilasser G, Fazilleau P and Tixador P 2017 Experimental measurement and numerical simulation of the screening current-induced field decay in a small ReBCO coil *IEEE Trans. Appl. Supercond* **27** 4900104.

[15] Ueda H, Fukuda M, Hatanaka K, Wang T, Ishiyama A and Noguchi S 2013 Spatial and temporal behavior of magnetic field distribution due to shielding current in HTS coil for cyclotron application *IEEE Trans. Appl. Supercond.* **23** 4100805.

[16] Hahn S, Kim K, Kim K. Hu X, Painter T, Dixon I, Kim S, Bhattarai K R, Noguchi S, Jaroszynski J and Larbalestier D C 2019 45.5-tesla direct-current magnetic field generated with a high-temperature superconducting magnet *Nature* **570** 496-9

[17] Hahn S, Kim K L, Kim K., Bhattarai K, Radcliff K, Hu X, Painter T, Dixon I and Larbalestier D 2018 Progress in No-Insulation HTS Magnet Researches *presented at Applied Superconductivity Conference 2018*

[18] Hu X, Small M, Kim K, Kim K, Bhattarai K, Polyanskii A, Radcliff K, Jaroszynski J, Bong U, Park J H, Hahn S and Larbalestier D 2020 Analyses of the plastic deformation of coated conductors deconstructed from ultra-high field test coils *Supercond. Sci. Technol.*, **33** 095012

[19] Takahashi S, Suetomi Y, Takao T, Yanagisawa Y, Maeda H, Takeda Y and Shimoyama J 2020 Hoop stress modification, stress hysteresis and degradation of a REBCO coil due to the screening current under external magnetic field cycling *IEEE Trans. Appl. Supercond.* **30** 4602607

[20] Berrospe-Juarez E, Trillaud F, Zermeño V M R and Grilli F 2020 Screening current-induced field and field drift study in HTS coils using *T-A* homogenous model *Journal of Physics: Conference Series* **1559** 012128

[21] Yan Y, Xin C, Guan M, Liu H, Tan Y and Qu Y 2020 Screening current effect on the stress and strain distribution in REBCO high-field magnets: experimental verification and numerical analysis *Supercond. Sci. Technol.* **33** 05LT02

[22] Kolb-Bond D, Bird M, Dixon I R and Painter T 2021 Screening current rotation effects: SCIF and strain in REBCO magnets *Supercond. Sci. Technol.* **34** 095004

[23] Wang Y, Bai H, Li J, Zhang M and Yuan W 2020 Electromagnetic modelling using T-A formulation for high-temperature superconductor (RE)$Ba_2Cu_3O_x$ high field magnets *High Voltage* **5** 218-26

[24] Mataira R C, Ainslie M D, Badcock R A and Bumby C W 2020 Finite-element modelling of no-insulation HTS coils using rotated anisotropic resistivity *Supercond. Sci. Technol.* **33** 08LT01

[25] Itoh R, Oga Y, Noguchi S, Igarashi H and Ueda H 2013 Numerical simulation of screening current distribution in HTS tape of high field magnet *Physica C* **484** 300-4

[26] Ueda H, Saito J, Ariya Y, Mochida A, Wang T, Wang X, Agatsuma K and Ishiyama A 2015

Reduction of irregular magnetic field generated by screening current in REBCO coil *IEEE Trans. Appl. Supercond.* **25** 6603205

[27] Noguchi S, Hahn S, Ueda H, Kim S and Ishiyama A 2018 An extended thin approximation method to simulate screening current induced in REBCO coils *IEEE Trans. Magn.* **54** 7201904

[28] Mifune T, Tominaga N, Sogabe Y, Mizobata Y, Yasunaga M, Ida A, Iwashita T and Amemiya N 2019 Large-scale electromagnetic field analyses of coils wound with coated conductors using a current-vector-potential formulation with a thin-strip approximation *Supercond. Sci. Technol.* **32** 094002

[29] Noguchi S, Imai T, Park D, Hahn S and Iwasa Y 2020 A simple screening current simulation method using equivalent circuit model for REBCO pancake coils *Supercond. Sci. Technol.* **33** 115005

[30] Berrospe-Juarez E, Zermoño V M R, Trillaud F and Grilli F 2019 Real-time simulation of large-scale HTS systems: multi-scale and models using the *T-A* formulation *Suerpcond. Sci. Technol.* **32** 065003

[31] Wang T, Noguchi S, Wang X, Arakawa I, Minami K, Monma K, Ishiyama A, Hahn S and Iwasa Y 2015 Analyses of transient behaviors of no-insulation REBCO pancake coils during sudden discharging and overcurrent *IEEE Trans. Appl. Supercond.* **25** 4603409

[32] Miyao R, Igarashi H, Ishiyama A and Noguchi S 2018 Thermal and electromagnetic simulation of multistacked no-insulation REBCO pancake coils on normal-state transition by PEEC method *IEEE Trans. Appl. Supercond.* **28** 4601405

[33] Markiewicz W D, Jaroszynski J J, Abraimov D V, Joyner R E and Khan A 2016 Quench analysis of pancake wound REBCO coils with low resistance between turns *Supercond. Sci. Technol.* **29** 025001

[34] Wang Y, Chan W K and Schwartz J 2016 Self-protection mechanism in no-insulation (RE)$Ba_2Cu_3O_x$ high temperature superconductor pancake coils *Supercond. Sci. Technol.* **29** 045007

[35] Nugteren J, Kirby G A, Rijk G, Rossi L, Kate H H J, and Dhall'e M M J 2015 Study of a 5 T research dipole insert-magnet using an anisotropic ReBCO roebel cable*IEEE Trans. Appl. Supercond.* **25** 4000705

[36] Nakata T, Takahashi N and Fujiwara K 1988 Efficient solving techniques of matrix equations for finite element analysis of eddy currents *IEEE Trans. Magn.* **24** 170-3

[37] Tsuboi H and Kunisue K 1991 Eddy current analysis of thin plates taking account of the source current distributions and its experimental verifications *IEEE Trans. Magn.* **27** 4020-3

[38] Hashizume H, Sugiura T, Miya K and Toda S 1992 Numerical analysis of electromagnetic phenomena in superconductors *IEEE Trans. Magn.* **28** 1332-5

[39] Hamada S and Takuma T 2003 Effective precondition technique to solve a full linear system for the fast multipole method *IEEE Trans. Magn.* **39** 1666-9

[40] Freengard L and Rokhlin V 1997 A new version of the fast multipole method for the Laplace equation in three dimensions *Acta Numerica* **6** 229-69

[41] Norris W T 1970 Calculation of hysteresis losses in hard superconductors carrying ac: Isolated conductors and edges of thin sheets *J. Phys. D, Appl, Phys.* **3** 489-507

[42] Noguchi S, Ueda H, Hahn S, Ishiyama A and Iwasa Y 2019 A simple screening current-induced magnetic field estimation method for REBCO pancake coils *Supercond. Sci. Technol.* **32** 045007

[43] Hahn S, Park D K, Bascuñán J and Iwasa Y 2011 HTS pancake coils without turn-to-turn insulation *IEEE Trans. Magn.* **21** 1592-5

[44] Wang X, Hahn S, Kim Y, Bascuñán J, Voccio J, Lee H and Iwasa Y 2013 Turn-to-turn contact characteristics for an equivalent circuit model of no-insulation ReBCO pancake coil *Supercond. Sci. Technol.* **26** 035012

[45] Noguchi S 2019 Electromagnetic, thermal, and mechanical quench simulation of NI REBCO pancake coils for high magnetic field generation *IEEE Trans. Appl. Supercond.* **29** 4602607

[46] Ueda H, Ishiyama A, Yuta A, Wang T, Wang X, Agatsuma K, Miyazaki H, Tosaka T, Nomura

S, Kurusu T, Urayama S and Fukuyama H 2015 Evaluation of magnetic-field distribution by screening current in multiple REBCO coils *IEEE Trans. Appl. Supercond.* **25** 4700705

[47] Ueda H, Imaichi Y, Wang T, Ishiyama A, Noguchi S, Iwai S, Miyazaki H, Tosaka T, Nomura S, Kurusu T, Urayama S and Fukuyama H 2016 Numerical simulation on magnetic field generated by screening current in 10-T-class REBCO coil *IEEE Trans. Appl. Supercond.* **26** 4701205

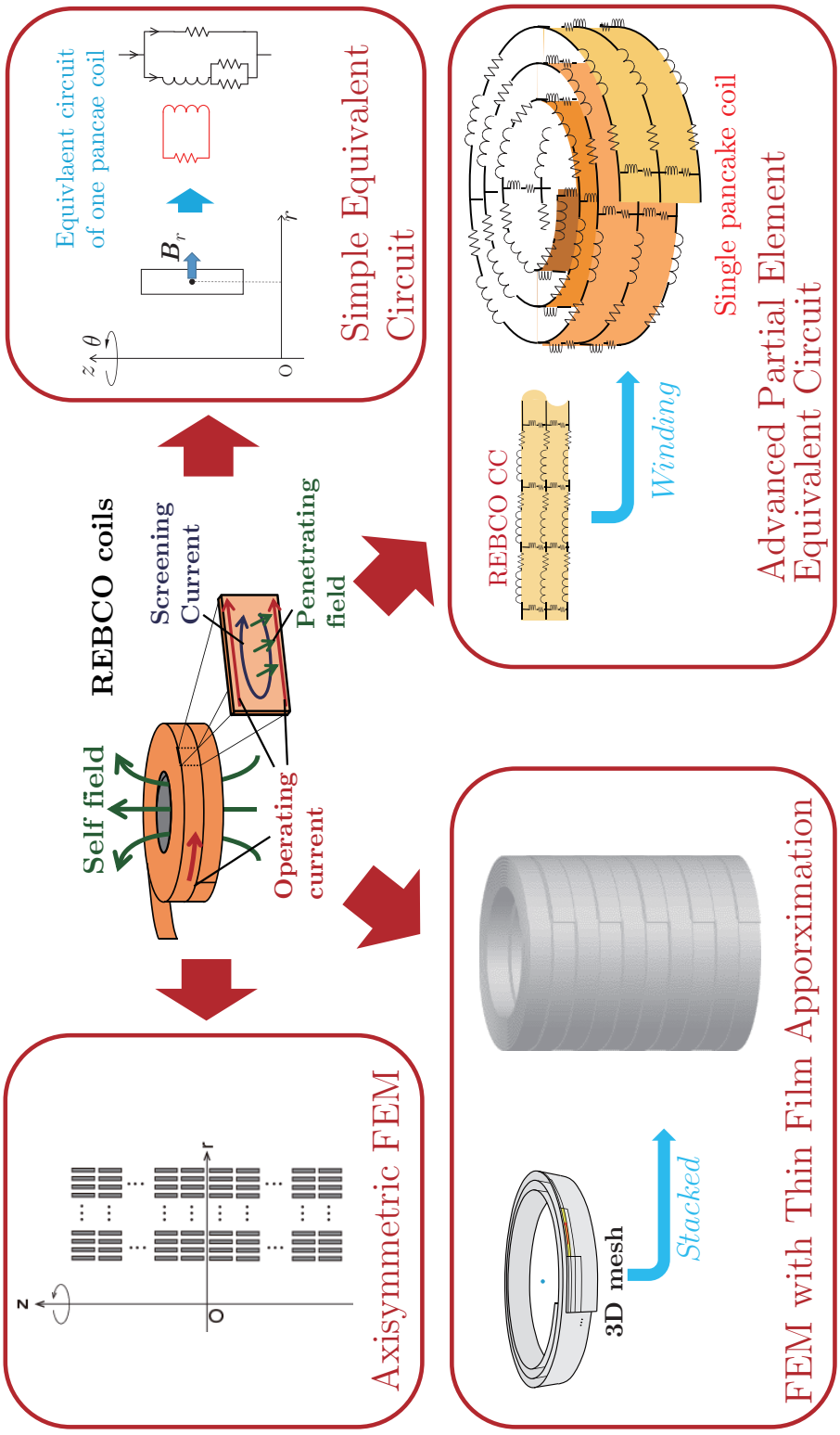


**Figure 1.** Key concepts of the four screening current (SC) simulation models.

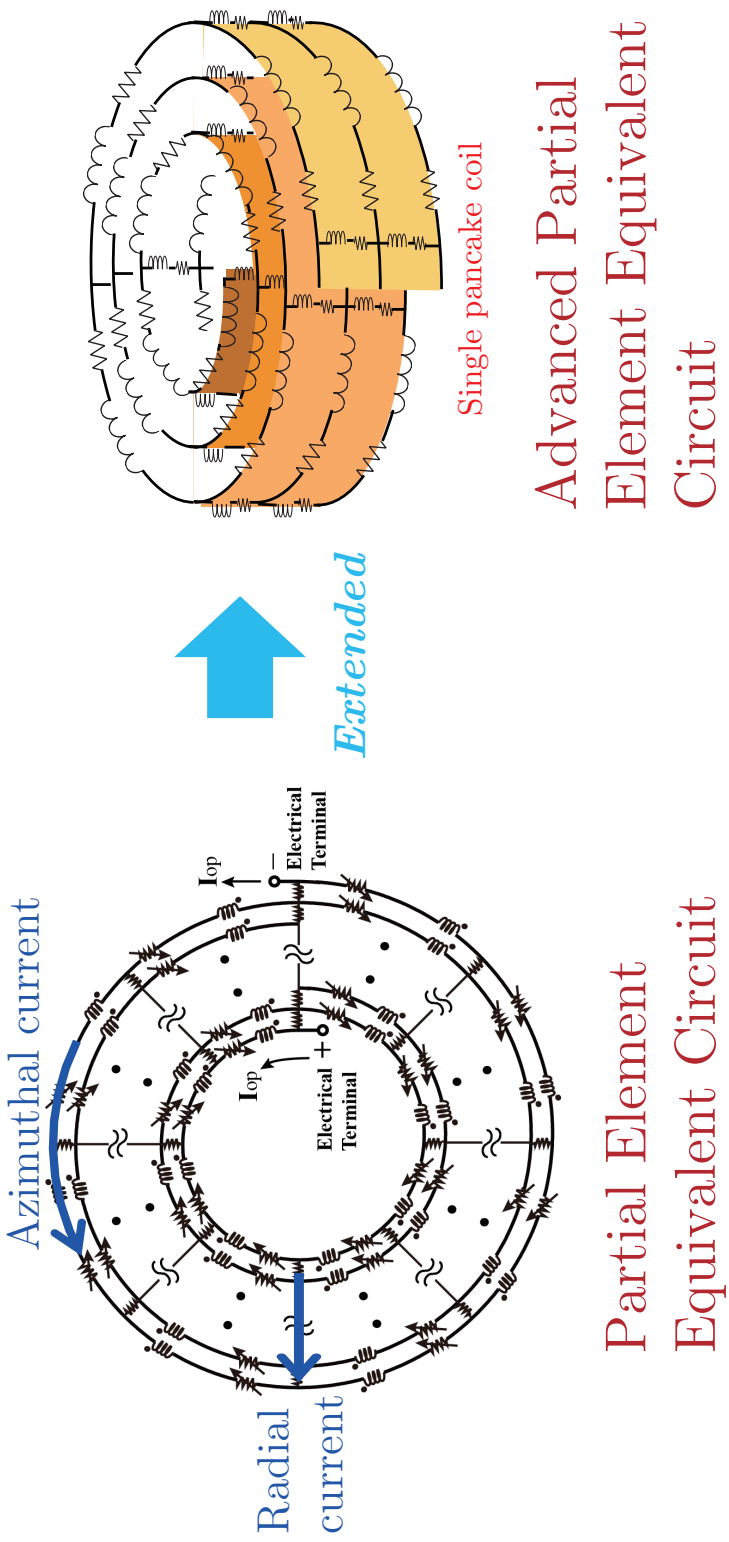


**Figure 2.** Proposed advanced partial element equivalent circuit (A-PEEC) model. By stacking the PEEC model in the REBCO tape width direction, the A-PEEC model is constructed.

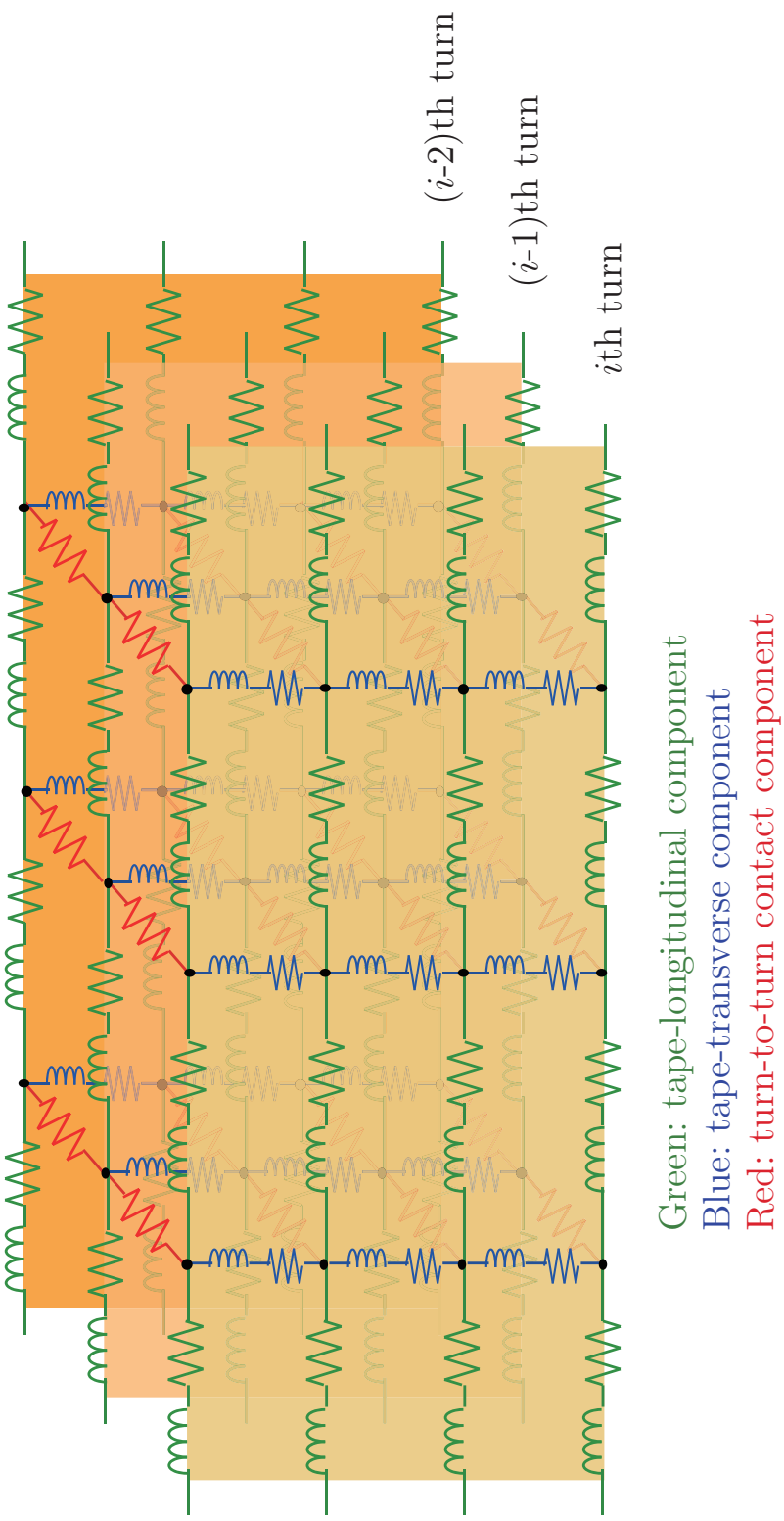


**Figure 3.** Local loops of equivalent circuit for A-PEEC model. This model can be extended to an NI pancake coil easily, by considering the turn-to-turn contact resistances. For an insulated REBCO pancake coil, the turn-to-turn contact resistances are omitted.

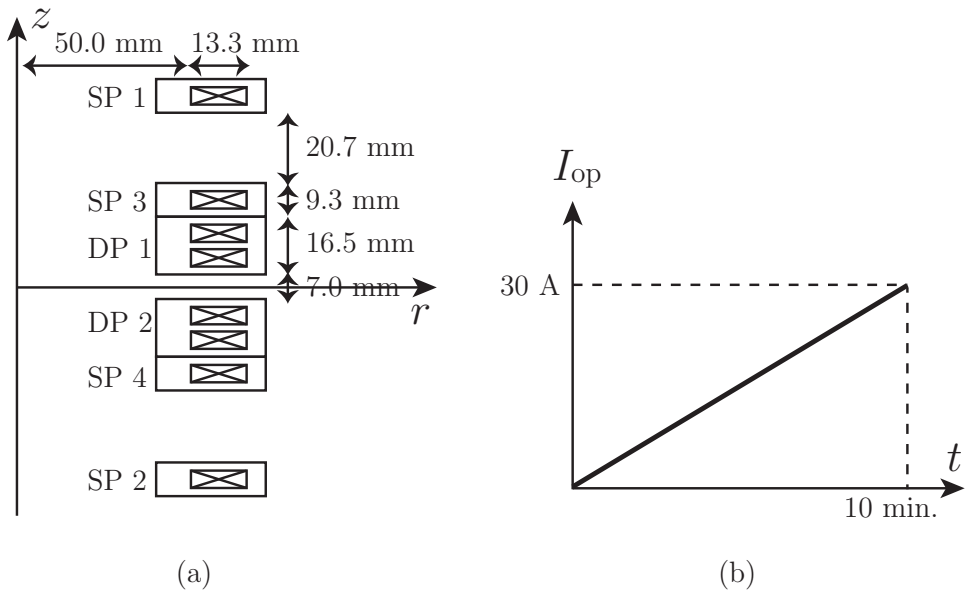


**Figure 4.** (a) Simulated 2 DP + 4 SP magnet configuration and (b) charging pattern.

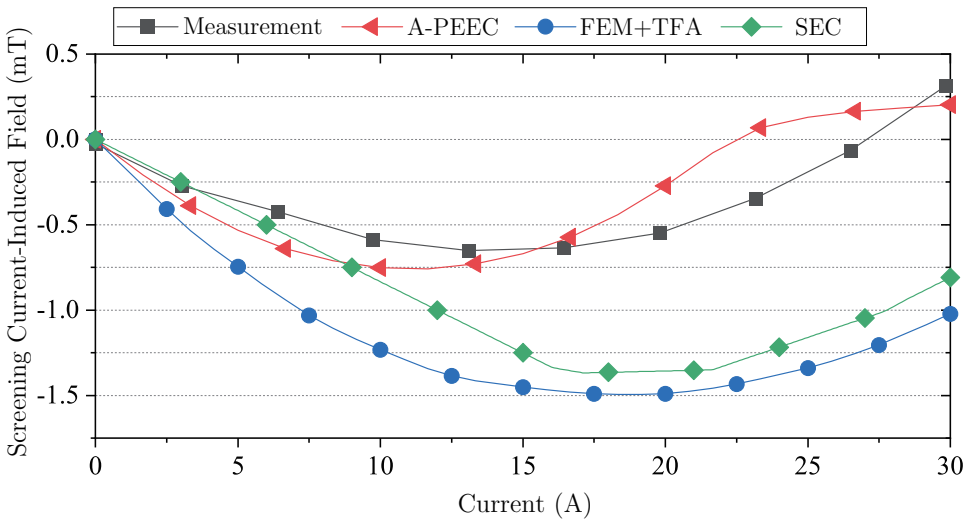


**Figure 5.** Screening current-induced fields simulated by A-PEEC, FEM + TFA, and SEC, and the measurement.

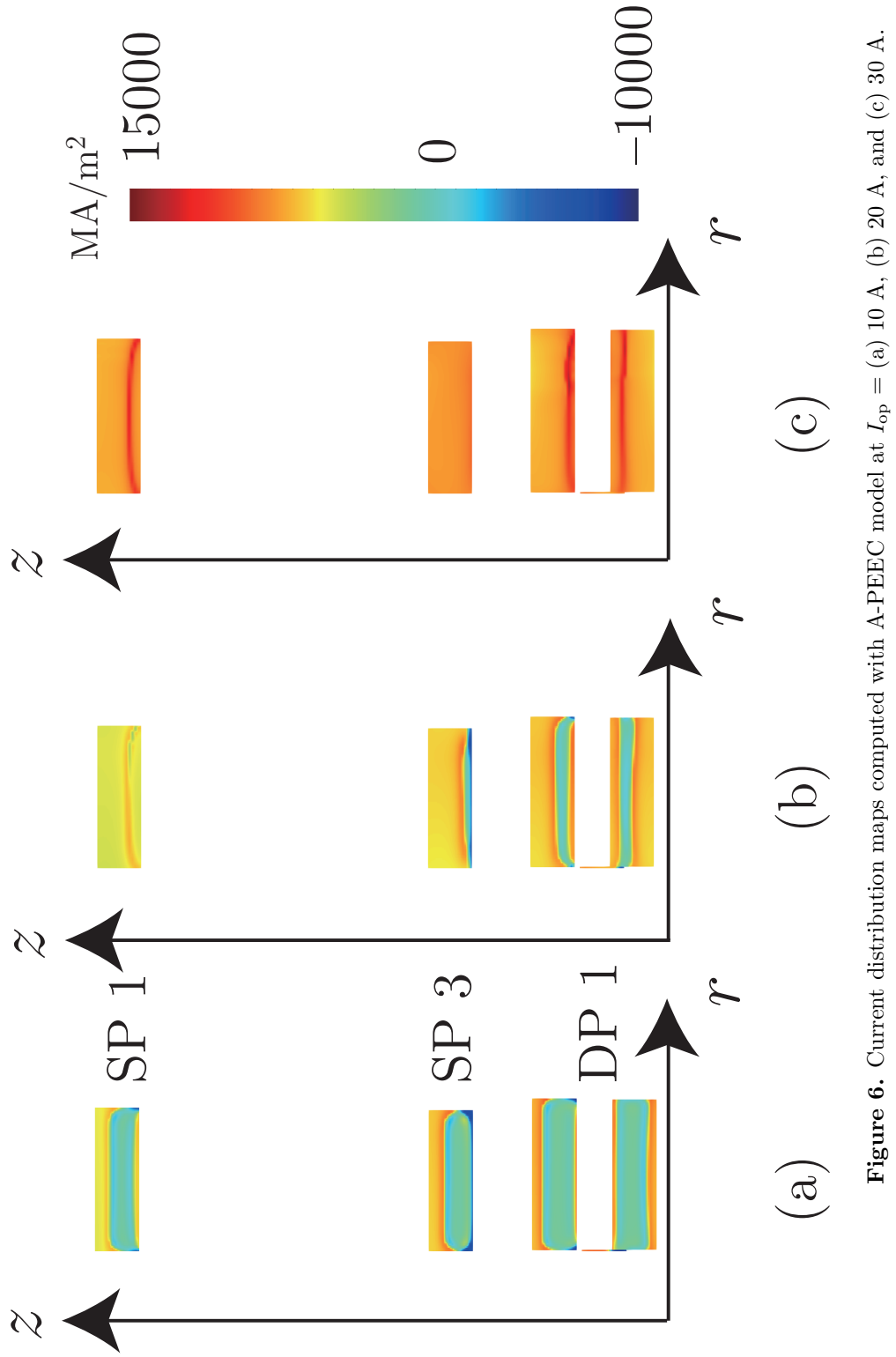


**Figure 6.** Current distribution maps computed with A-PEEC model at $I_{\mathrm{op}}$ = (a) 10 A, (b) 20 A, and (c) 30 A.

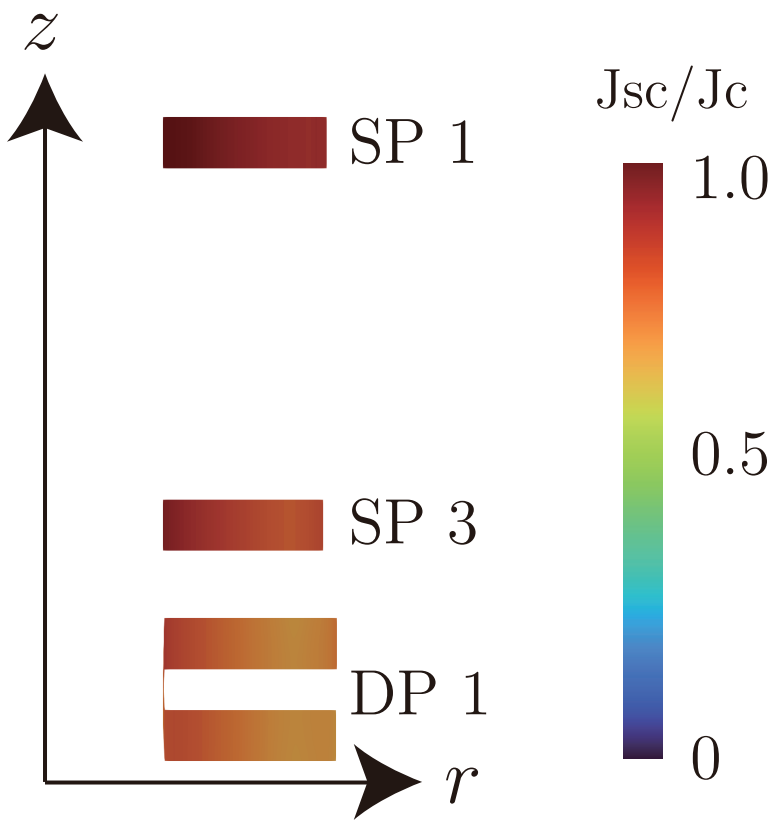


**Figure 7.** Ratio of screening current density $J_{sc}$ to critical current density $J_c$ computed with A-PEEC model at $I_{\mathrm{op}} = 30$ A.

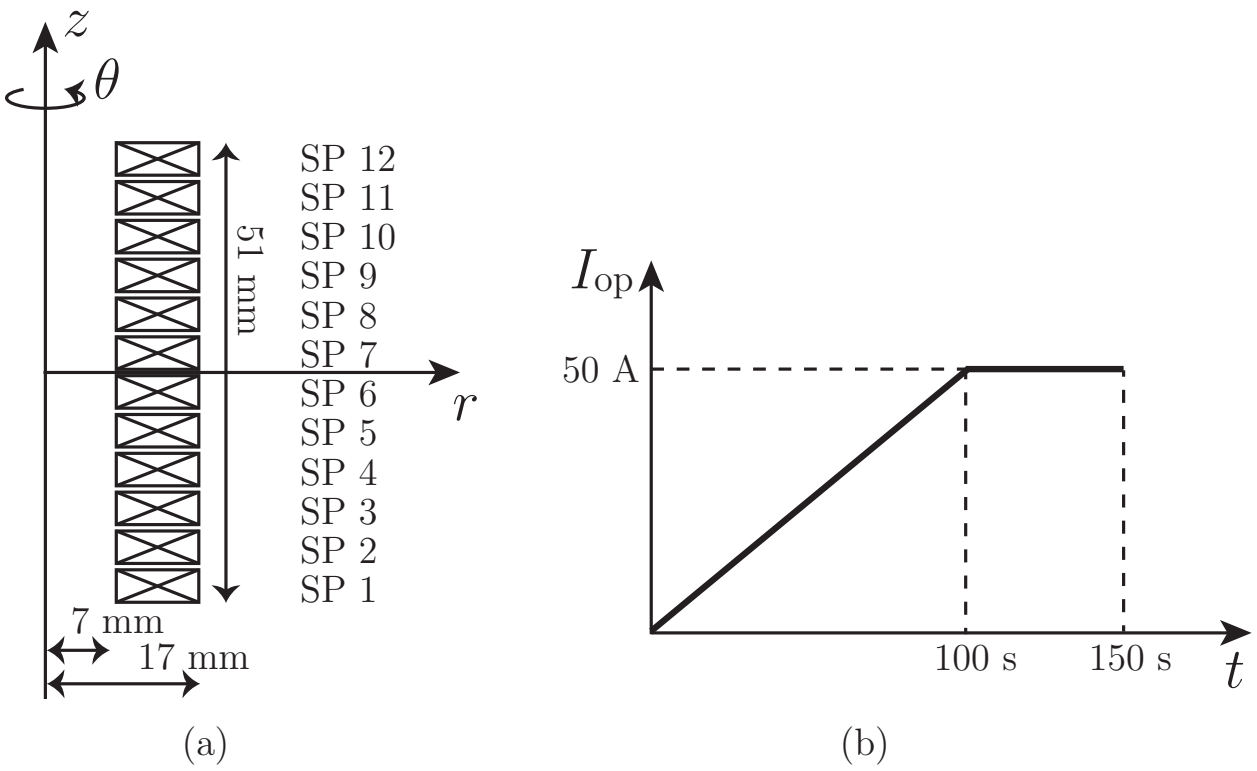


**Figure 8.** (a) LBC3 magnet configuration and (b) charging pattern.

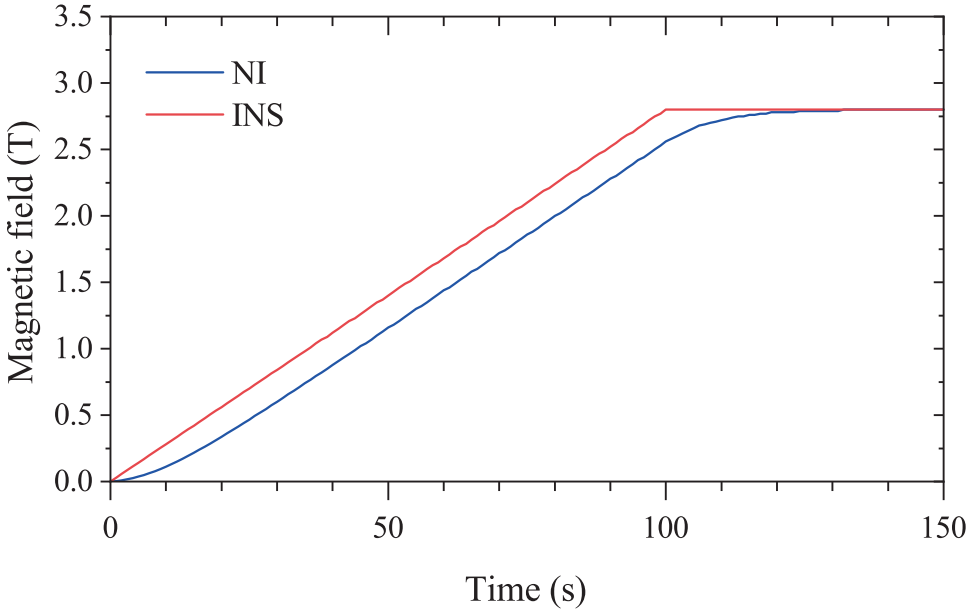


**Figure 9.** Axial magnetic field at magnet center in cases of turn insulation (INS) and no-insulation (NI).

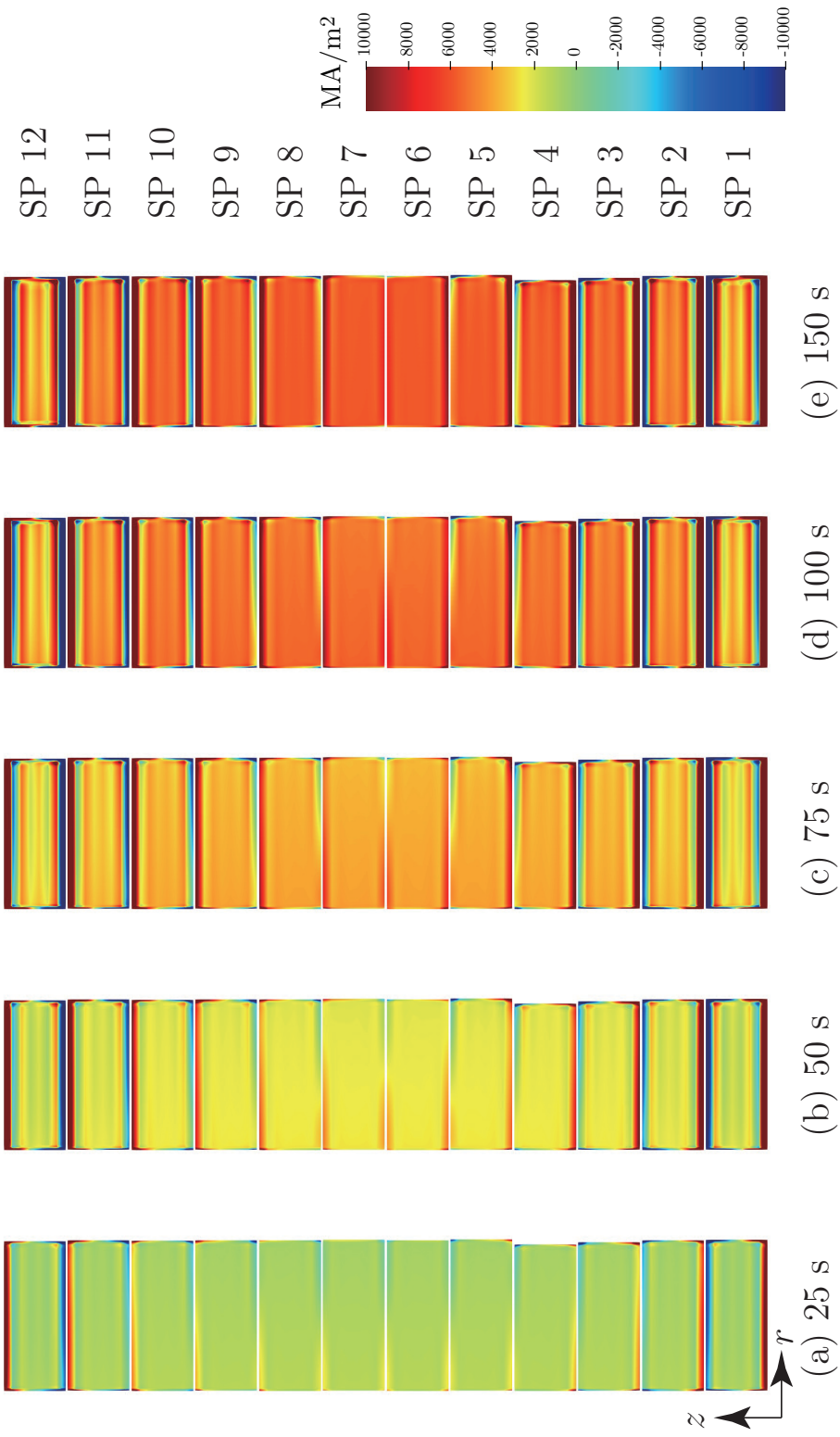


**Figure 10.** Screening current distribution map in cases of no-insulation (NI). The average current density in the REBCO layer thickness direction is depicted.

**Table 1.** Key features of SC computation models.

| | |
|---|---|
| Axi-FEM | · Inaccurate due to homogenization method<br>· Short computation time and small memory usage<br>· Unable to consider time-varying $z$-field correctly in (2) |
| FEM+TFA | · Accurate, but long comp. time & huge memory usage<br>· Axial current and wincing structure are taken into account<br>· Unable to consider time-varying $z$-field correctly |
| SEC | · Very simple, but inaccurate<br>· Time-varying $z$-field is correctly simulated<br>· Extendable to NI coils |
| A-PEEC | · Accurate, but not easy to calculate inductances<br>· Axial current and winding structure are taken int account<br>· Extendable to NI coils |

**Table 2.** Specifications of 2 DP + 4 SP magnet & simulation conditions.

| | |
|---|---|
| REBCO tape | SuperPower SCS4050-AP |
| Tape width | 4.0 mm |
| Tape Thickness | 0.1 mm |
| Inner radius | 50.0 mm |
| Avg. outer radius | 63.3 mm |
| Turn-to-turn insulation | Kapton 25 $\mu$m |
| Coolant | Liquid nitrogen |

| Coil | Coil $I_c$ (A) | $n$ value |
|---|---|---|
| SP 1 | 41.4 | 22.0 |
| SP 2 | 41.4 | 25.4 |
| SP 3 | 51.1 | 23.5 |
| SP 4 | 48.9 | 23.1 |
| DP 1 | 53.2 | 26.1 |
| DP 2 | 53.8 | 28.8 |

**Table 3.** Outline specifications of LBC3 & simulation conditions.

| | |
|---|---|
| Number of pancake coils | 12 |
| REBCO tape width | 4.03 mm |
| REBCO tape Thickness | 0.045 mm |
| Inner radius | 7.0 mm |
| Avg. outer radius | 17.0 mm |
| Avg. number of turns | 220 |
| Coolant | Liquid helium |

**Table 4.** Measured axial field and screening current-induced field at magnet center.

| Current $I_{op}$ | Measured field $B_0$ | Measured SC field $B_{sc}$ |
|---|---|---|
| 8.96 A | 0.51 T | 0.02 T |
| 48.9 A | 2.59 T | 0.29 T |